

## Radiation properties of IR calibrators with V-grooved surfaces

Alexander V. Prokhorov, Leonard M. Hanssen\*, Sergey N. Mekhontsev  
National Institute of Standards and Technology, 100 Bureau Dr., Gaithersburg,  
MD 20899-8441, USA

### ABSTRACT

Use of linear or concentric grooves is a well-known approach for increasing the surface emissivity to enable the construction of compact blackbody radiators, improve absorptance of stray radiation traps, baffles and thermal radiation detectors, as well as enhance thermal radiation transfer. Emitters with V-grooved surfaces are widely used as reference sources in radiation thermometry and radiometry. In the design phase of such devices, it is important to predict their performance. Most existing models are devoted to modeling isothermal linear grooves with purely diffuse or specular reflectance. Radiation behavior of concentric grooves differs from linear ones and becomes similar only for large values of the ratio of the radial coordinate to the groove period. This paper covers numerical modeling of isothermal and non-isothermal concentric grooves with mixed specular-diffuse reflection for various viewing conditions using Monte Carlo specialized software. It is shown that the temperature drop towards the peak of a groove might lead to a substantial decrease of the grooves' effective emissivity.

**Keywords:** emissivity, blackbody radiators, concentric grooves, specular-diffuse reflection, Monte Carlo method.

### 1. INTRODUCTION

Parallel rectilinear or annular concentric grooves of various profiles are widely used to enhance radiation heat transfer, to improve the absorptance of stray radiation traps, baffles and thermal radiation detectors, to increase the emissivity of blackbody radiators, especially compact spaceborne calibrators<sup>1,2</sup>. The effective (or apparent) emissivity of grooved structure is greater than the emissivity of flat surface due to multiple reflections among groove walls; it can approach unity, i.e. the emissivity of a perfect blackbody. In radiometry<sup>3-5</sup> and radiation thermometry<sup>6</sup>, such radiators serve as reference sources. In their design stage, it is necessary to be able to predict their performance.

There are several studies dedicated to the modeling of a rectilinear groove with purely diffuse or purely specular reflectance. Daws<sup>7</sup> analyzed the angular emission properties for a rectilinear groove with an isosceles triangular profile and isothermal diffuse walls based on approximate expressions for directional and hemispherical effective emissivity. Sparrow and Lin<sup>8</sup> considered the absorption of thermal radiation in purely specular and purely diffuse V-grooves for collimated and hemispherical irradiation. Their results can be applied to an emitting groove by using the reciprocity principle and Kirchhoff's law. Sparrow and Gregg<sup>9</sup> obtained numerical solutions of Fredholm's integral equations of the 2<sup>nd</sup> kind, which describe the radiation heat exchange in an infinite groove with a rectangular profile. Psarouthakis<sup>10</sup> derived a useful analytical formula for effective emissivity of an isothermal diffuse triangular groove. Perlmutter and Howell<sup>11</sup> examined the directional radiation properties of diffuse grooves having triangular and trapezoidal profiles. O'Brien and Heckert<sup>12</sup> obtained an exact solution for the effective emissivities of isothermal and non-isothermal specular grooves with a triangular shape. They also found an approximate numerical solution for both isothermal and non-isothermal diffuse grooves. Isothermal specular V-grooves were also studied by Zipin<sup>13</sup>. Kelly<sup>14</sup> derived an important analytical expression for the local effective emissivity at the vertex of an isothermal diffuse V-groove. Zhimin<sup>15</sup> proposed an approximate solution of an integral equation describing radiative heat transfer in both isothermal and non-isothermal diffuse rectilinear grooves with a triangular shape and obtained the dependences of total directional, normal, and hemispherical emissivities on several critical parameters.

The radiation properties of ringed grooves differ from those associated with rectilinear parallel grooves (e.g. when comparing ray trajectories at oblique viewing of rectilinear and annular grooves of triangle section with specularly

---

\* [hanssen@nist.gov](mailto:hanssen@nist.gov); phone: 301-975-2344; fax: 301-840-8551; www.nist.gov

reflecting walls) and become similar only at large values of the ratio of the radial coordinate to the groove period, where the curvature of the annular grooves tends to zero. However, there is a lack of work devoted to annular concentric grooves. In order to bridge this gap, we performed a numerical study<sup>16</sup> of radiation characteristics of concentric V-grooves. A simple specular-diffuse model of reflection was used for the groove walls. According to this model, the directional-hemispherical reflectance does not depend on the incidence angle of radiation. This condition is often violated, particularly for grazing incidence that can take place for viewing a surface with concentric V-grooves along the groove's rotation axis. In this paper, we will employ a more realistic model of reflection and compare the results obtained by using both models.

## 2. COMPUTATIONAL ALGORITHM DESCRIPTION

### 2.1. Specular-diffuse model of reflection

According to the specular-diffuse (SD) model, the radiation properties of a surface can be specified by a directional-hemispherical reflectance  $\rho = 1 - \varepsilon$ , where  $\varepsilon$  is the hemispherical emissivity, and a diffusivity (not to be confused with diffusivity)  $D$ , defined as the ratio of the diffuse component of reflectance to the total reflectance. Diffusivity can be an arbitrary function of incident angle, but the inequality  $0 < D < 1$  must be obeyed, and  $\rho$  must be independent of incident angle. Unless stated otherwise, we will deal with spectral quantities.

For most real-world materials, the specular component of reflection and the directional-hemispherical reflectance both increase with incident angle.

### 2.2. Fresnelian-Lambertian model of reflection

The Fresnelian-Lambertian (FL) model of reflection represents the spectral directional-hemispherical reflectance in the form of the sum of an angle-independent perfectly diffuse (Lambertian) component and a specular Fresnelian component that depends on incidence angle  $\theta$ :

$$\rho(\lambda, \theta) = d \cdot R_d(\lambda) + (1 - d) \cdot F(n(\lambda), k(\lambda), \theta), \quad (1)$$

where  $d$  is a diffuse factor (weighting multiplier),  $R_d(\lambda)$  is a partial spectral diffuse reflectance (hence  $d \cdot R_d(\lambda)$  is the diffuse component of reflectance),  $n$  and  $k$  are the optical constants of the material (refraction index and extinction coefficient), and  $\lambda$  is the wavelength. A non-polarized radiation Fresnel's function can be written in the form

$$F(n, k, \theta) = \frac{1}{2} \frac{(a - c)^2 + b^2}{(a + c)^2 + b^2} \left[ \frac{(a + c - 1/c)^2 + b^2}{(a - c + 1/c)^2 + b^2} + 1 \right], \quad (2)$$

where  $c = \cos \theta$ ,

$$a^2 = \frac{1}{2} \left( \sqrt{(n^2 - k^2 + c^2 - 1)^2 + 4n^2k^2} + n^2 - k^2 + c^2 - 1 \right), \quad (3)$$

and

$$b^2 = \frac{1}{2} \left( \sqrt{(n^2 - k^2 + c^2 - 1)^2 + 4n^2k^2} - n^2 + k^2 - c^2 + 1 \right). \quad (4)$$

Hereafter, we will consider the single wavelength case and omit the symbol  $\lambda$  for simplicity.

The diffusivity  $D$  for the FL model depends on incidence angle:

$$D(\theta) = \frac{d \cdot R_d}{d \cdot R_d + (1-d) \cdot F(n, k, \theta)} \quad (5)$$

The FL model can be obtained by considering a surface consisting of two types of areas: (1) Lambertian, yielding a relative total contribution  $d$  of the total area, and (2) Fresnelian with a total contribution  $1 - d$ . The individual areas should be small in comparison with the entire irradiated area and intermixed randomly. The directional-hemispherical reflectance  $\rho$  can be considered as the quantity averaged over the entire irradiated area, and  $R_d, n, k$  as the local characteristics of areas of the two types.

The parameters  $d, R_d, n, k$  of the FL model can be determined if the values of the directional-hemispherical reflectance are measured for at least four values of incidence angle. If the measurements are performed for more than 4 incidence angles, the least square method can be applied to solve the following system of linear equations:

$$\rho(\theta_j) = d \cdot R_d + (1-d) \cdot F(n, k, \theta_j), \quad j \geq 4. \quad (6)$$

The computed values of  $n$  and  $k$  should be considered as only best-fit values and do not need to be coincident with the real refraction index and extinction coefficient of a material.

### 2.3. Computational model and method

We applied the STEEP3<sup>17\*</sup> code to the numerical modeling of grooved surfaces. This code, which employs the Monte-Carlo method, is described in a series of papers<sup>18-20</sup>. It is designed to compute the spectral and total effective emissivity of cavities formed by rotation of non-self-crossing polygonal lines around any axis. For each surface of revolution, an arbitrary temperature distribution and specular-diffuse reflectance can be assigned. The code was customized to operate with the FL model of reflection to our specification.

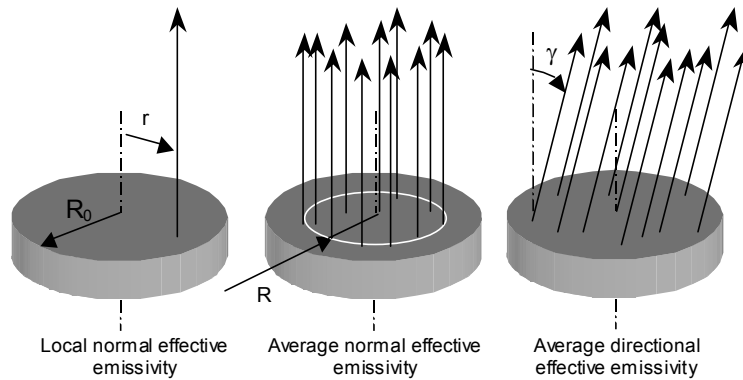


Figure 1. Viewing conditions for different types of effective emissivity.

\* Certain commercial software is identified in this paper in order to specify the computational procedure adequately. Such identification is not intended to imply recommendation or endorsement by the National Institute of Standards and Technology, nor is it intended to imply that the software identified are necessarily the best available for the purpose.

The viewing conditions for the three most important types of effective emissivity are shown schematically in Figure 1. Their definitions are given below.

The *spectral local directional effective emissivity* is defined as the ratio of the spectral radiance for a given location, wavelength, temperature, and direction to the spectral radiance of a perfect blackbody for the same wavelength, temperature, and direction. This is a primary radiation characteristic; all other types of effective emissivities can be obtained by averaging over a spectral range, solid angle, and/or viewed area.

The *local normal effective emissivity* corresponds to observation along a ray, which is parallel to the radiator axis. The *average normal effective emissivity* is applicable to a case when a detector of radius  $R$  is coaxial with the radiator and located at an infinite distance from it. The *average directional effective emissivity* corresponds to the observation of parallel rays at an angle  $\gamma$ .

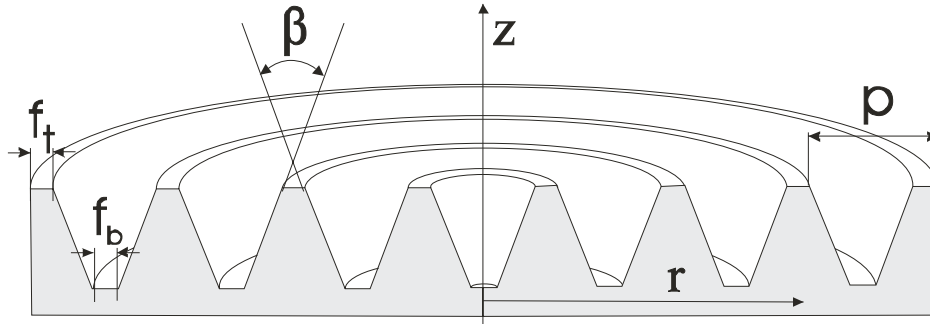


Figure 2. Geometrical model of the radiator:  
 $p$  is the pitch,  $f_t$  and  $f_b$  are the widths of the flat areas at the top and bottom, and  $\beta$  is the included angle.

We study radiators with concentric grooves of trapezoidal profile as depicted in Figure 2. The geometric parameters of this structure are the following:  $p$  is the pitch (or period),  $f_t$  and  $f_b$  are the widths of the flat areas at the top and bottom, and  $\beta$  is the angle between lateral sides of the trapezoid. The groove shape becomes triangular if  $f_t = f_b = 0$ . We assume that the center of the radiator is always concave. To ensure the comparability of the results obtained with the use of both the SD and FL reflection models, we selected a pair of datasets with the following characteristics:  $\rho_{SD} = \rho_{FL}(n, k, 0) = 0.7$ ;  $D_{SD} = D_{FL}(n, k, 0) = 0.5$ . To equate the specular component of the FL model at normal incidence to the specular component of the SD model, we chose  $n = 2.2$  and  $k = 1.53$  from data for various graphite samples<sup>21,22</sup> at  $10.6 \mu\text{m}$ . The appropriate angular dependences for the FL model are shown in Figure 3. Hereafter we will designate the results obtained for these datasets by the labels “SD” and “FL”.

### 3. ISOTHERMAL GROOVES

#### 3.1 Local and average normal effective emissivities of triangular grooves

Figure 4 shows the calculated distribution of the local effective emissivity for isothermal diffuse triangular grooves as a function of the dimensionless radial coordinate for triangular grooves with unit period and three values of the angle  $\beta$  at the groove vertices. The local effective emissivity reaches a maximum at the groove bottoms and monotonically decreases towards the groove peaks. The use of a radiometer with a finite field of view (FOV) to scan the radiator along its diameter would flatten these oscillations.

For Figures 5 and 6, we modeled a radiator with a radius  $R_0 = 50$  relative linear units, and the number of triangular grooves determined by the angle at their apices. In Figure 5, the normal effective emissivity of an isothermal purely diffuse radiator with triangular concentric grooves is shown as a function of the visible area radius for three values of the angle  $\beta$  and for a wall emissivity of 0.7. The normal effective emissivity (averaged over viewing area) changes

according to the law of damped oscillations with increasing viewing area. The effect can be explained by the alternation of peak-adjacent and valley-adjacent regions of the groove as a boundary of the viewing area. In the limiting case of infinitely large viewing radius (and, therefore, zero curvature of surfaces forming the groove), it asymptotically approaches the effective emissivity of linear parallel grooves.

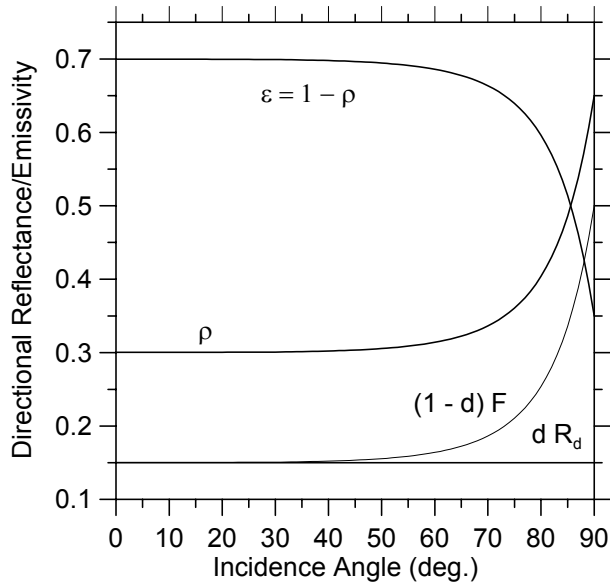


Figure 3. Components of the FL model for graphite.

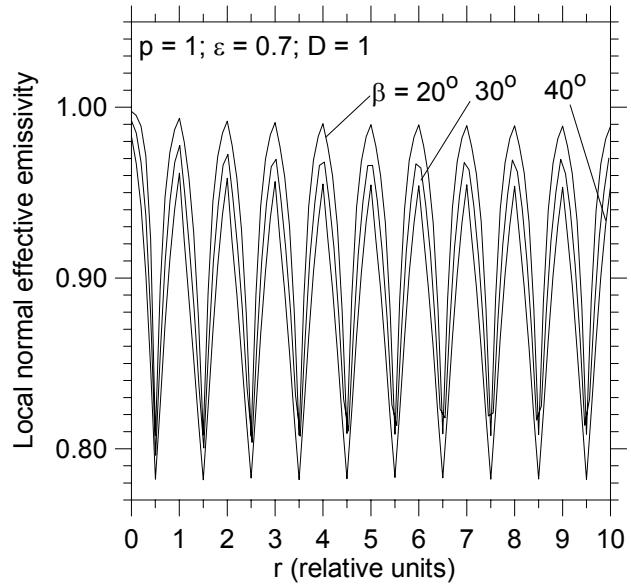


Figure 4. Distributions of local normal effective emissivities for perfectly diffuse grooves with  $\beta$ : 20°, 30° and 40°

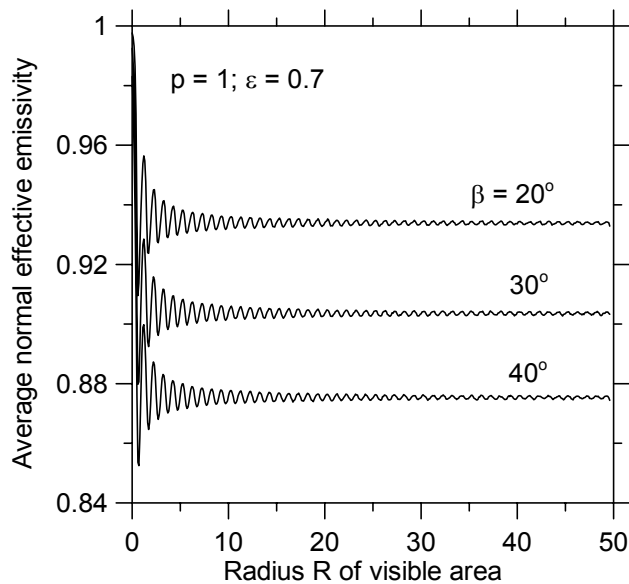


Figure 5. Average normal effective emissivity as a function of the visible area radius R for three values of the angle  $\beta$  at the vertex of triangular grooves

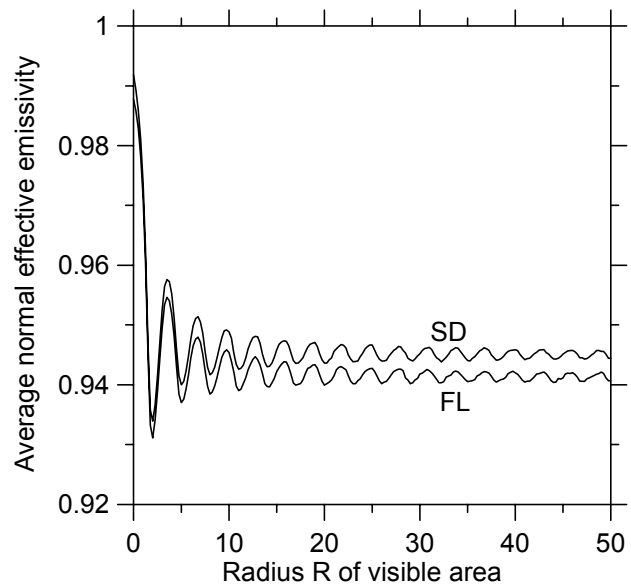


Figure 6. Average normal effective emissivity as a function of the visible area radius R for  $\beta = 30^\circ$  computed for the SD and FL models

The average normal effective emissivity as a function of the visible area radius  $R$  computed by using the SD and FL models for  $\beta = 30^\circ$  is depicted in Figure 6. The curve for the FL model lies about 0.003 below the SD curve because the FL model exhibits a lower emissivity, at large angles to the normal of the groove wall, than the SD model. Hence, this difference should decrease with increasing angle  $\beta$  at the groove vertex.

The dependences depicted in Figures 5 and 6 show that viewing a small number of concentric grooves may lead to poor repeatability of measurements due to any variability of alignment.

### 3.2 Normal average emissivity as a function of groove apex angle

Within the framework of the SD model, we performed numerical experiments to study the interrelationships between the wall emissivity, diffusivity, groove apex angle and normal effective emissivity. For plots in Figures 7 and 8, the entire radiator is viewable, and  $R = R_0 = 50$ .

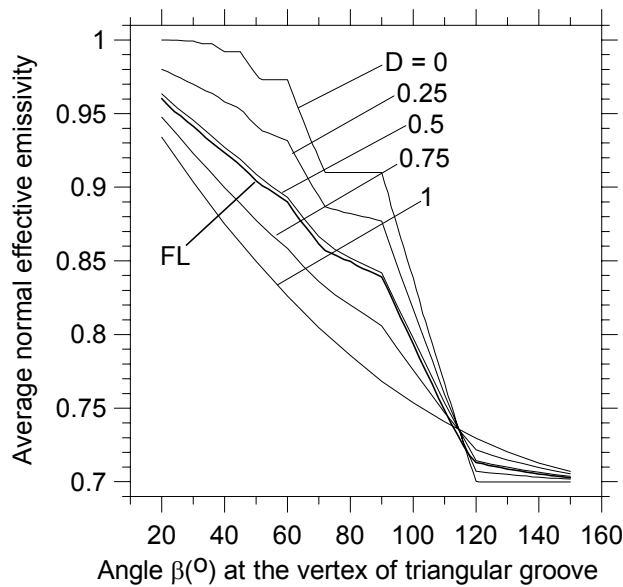


Figure 7. The normal effective emissivity of isothermal triangular ( $f_t = f_b = 0$ ) grooves vs. angle  $\beta$  computed by using the SD reflection model for  $\epsilon = 0.7$  and various  $D$ , and by using the FL model. For all cases;  $R = R_0 = 50$ .

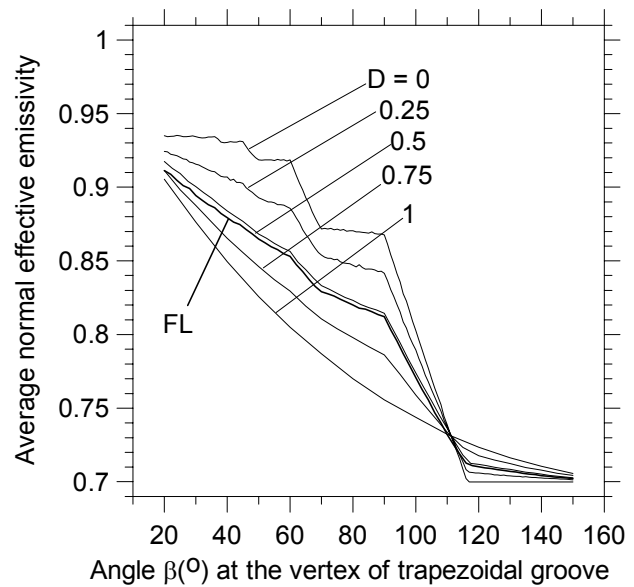


Figure 8. The normal effective emissivity of isothermal trapezoidal ( $f_t = f_b = 0.1$ ) grooves vs. angle  $\beta$  computed by using the SD reflection model for  $\epsilon = 0.7$  and various  $D$ , and by using the FL model. For all cases  $R = R_0 = 50$ .

Figures 7 and 8 illustrate the effects of introducing a specular component into the reflectance for a groove wall emissivity  $\epsilon = 0.7$  and several values of diffusivity  $D$ . The curves in Figure 7 are for triangular grooves ( $f_t = f_b = 0$ ) and in Figure 8 for trapezoidal grooves ( $f_t = f_b = 0.1$ ). For purely specular reflection, the dependence of the normal effective emissivity on the angle  $\beta$  is stepped due to the step change in the number of reflections. The presence of a diffuse component leads to a decrease in the effective emissivity for  $\beta$  less than about  $115^\circ$ . For  $\beta$  greater than this value, the inversion of curve order is observed. Due to the lower values of local emissivities of flat areas, the normal effective emissivity of trapezoidal grooves is lower compared to the corresponding values of emissivity for triangular grooves.

The dependences of the average normal effective emissivity on the vertex angle of triangular ( $f_t = f_b = 0$ ) and trapezoidal ( $f_t = f_b = 0.1$ ) grooves computed for the FL model of reflection are also depicted in Figures 7 and 8. The effective emissivities computed for the FL model are slightly ( $\sim 0.005$ ) lower than that for SD model at  $D = 0.5$ .

Curves in Figure 9 show the dependence of the normal effective emissivity on the angle  $\beta$  at the vertex of the perfectly diffuse ( $D = 1$ ) triangular grooves for surface emissivity 0.7, 0.8, 0.9, 0.95 and 0.98.

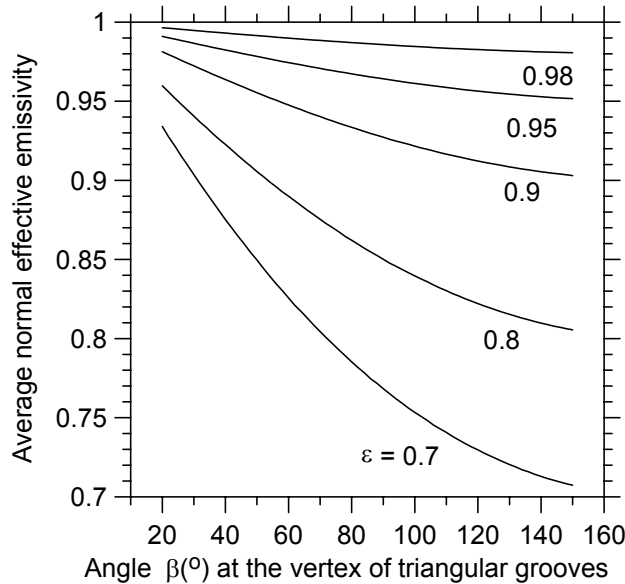


Figure 9. Average normal effective emissivity as a function of the angle  $\beta$  at the vertex of diffuse triangular grooves for five values of surface emissivity  $\varepsilon$  and  $R = R_0 = 50$ .

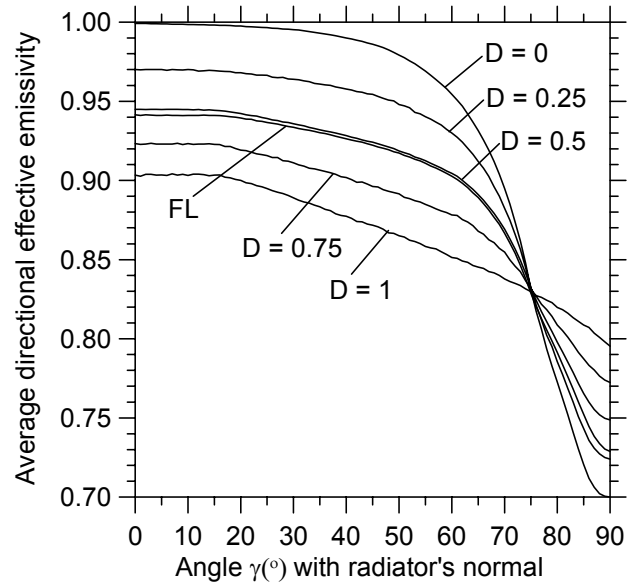


Figure 10. Dependence of the average directional effective emissivity of isothermal  $30^\circ$  triangular grooves on the angle of view  $\gamma$  computed by using the SD reflection model for  $\varepsilon = 0.7$  and several values of diffusivity  $D$ , and by using the FL model.  $R = R_0 = 50$ .

### 3.3 Directional effective emissivity

The angular properties of isothermal radiators with concentric triangular grooves have been examined within framework of the SD model. The computed dependence of the average directional emissivity for  $\beta = 30^\circ$  and  $\varepsilon = 0.7$  are depicted in Fig. 10. It is interesting to note that all curves in Figure 10 intersect at a single point where  $\gamma = \pi - \beta/2 = 75^\circ$ . This direction coincides with the normal to the groove wall. One can prove that for any specular component, the radiance (and, therefore, effective emissivity) of a groove wall in this direction must be the same.

For values of diffusivity  $D = 0$  to 1, the effective emissivity decreases with increasing viewing angle  $\gamma$ , i.e. the angle with respect to the normal to the flat surface of the radiator (prior to groove machining). All curves have a salient point (abrupt change of curvature) where  $\gamma = \beta/2$ . For the groove geometry considered, this corresponds to the onset of the “masking effect” when the observer ceases to collect radiation from one of the groove walls. The average directional effective emissivity of the same radiator, but computed by using the FL model is also depicted in Figure 10. The results obtained for the FL model are up to 0.005 lower than that for the SD model at  $D = 0.5$ .

## 4. NONISOTHERMAL GROOVES

In real radiators, the heat loss due to radiation from the groove walls leads to a temperature gradient along the groove depth. In the case where the temperature of the environment is lower than that of the radiator, peaks will be colder than valleys. In Figure 11, the computed spectral normal effective emissivity of  $30^\circ$  triangular V-grooves with diffuse gray walls (emissivity is 0.7) is shown for several values of linear temperature decrease toward the groove vertices. The temperature of the groove bases is selected to be 1000 K. We have chosen the temperature of the groove bottoms as the reference temperature (i.e. the temperature at which Planck’s function is computed).

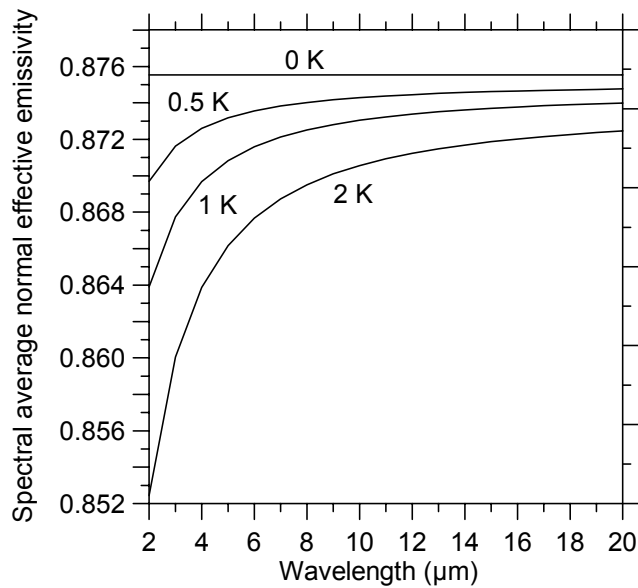


Figure 11. Spectral average normal effective emissivity of 30° triangular diffuse V-grooves (wall emissivity is 0.7) for 4 values of linear temperature decrease toward the groove vertices (0 K, 0.5 K, 1 K, and 2 K). Temperature of the groove bases is 1000 K.

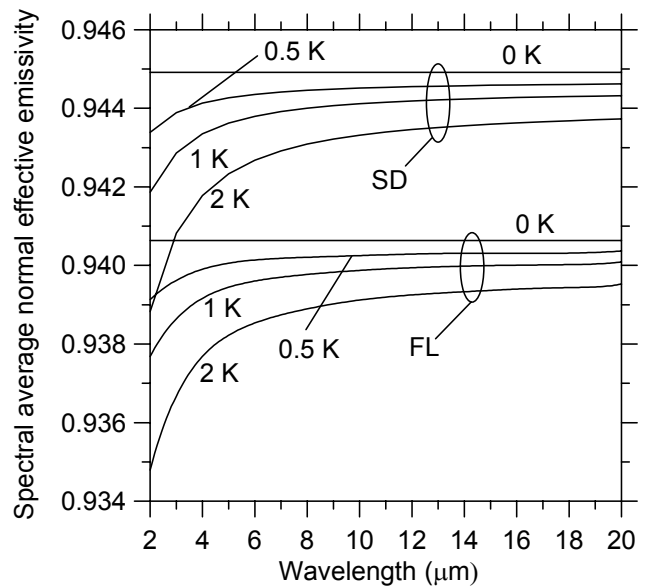


Figure 12. Spectral average normal effective emissivity of 30° triangular V-grooves computed using the SD and the FL reflectance models for 4 values of linear temperature decrease toward the groove vertices (0 K, 0.5 K, 1 K, and 2 K). Temperature of the groove bases is 1000 K.

In Figure 12, the spectral average normal effective emissivity of 30° triangular V-grooves computed using the SD and the FL reflectance models is shown for the same four temperature distributions as in Figure 11. The presence of a specular component of reflection leads to a substantial increase of the effective emissivity for both reflection models as compared to purely diffuse case depicted in Figure 11. The spectral curves computed for the SD and the FL models are quite similar but the values of effective emissivity obtained for the FL model are about 0.005 lower than those for the SD model.

## 5. CONCLUSIONS

The analysis of the results of the numerical experiments suggests the following:

1. The effective emissivity of calibration radiators with concentric grooves can be computed by the Monte Carlo method using either of the two (SD and FL) reflection models developed. Although the FL model is more realistic, it requires having sufficient experimental data to fit model parameters. The simpler SD model can be applied when the necessary experimental data is absent. For V-grooved structures, the SD model produces lower values of effective emissivities than the FL model for comparable parameters.
2. Evaluation of the uncertainties due to the effects of variations in the radiation properties of the groove walls, temperature gradients, manufacturing artifacts (such as surface irregularity), alignment of the FOV etc. can be undertaken within the framework of both models, through variation of all parameters.
3. The results obtained can be helpful to a user to predict the performance of specular/diffuse surfaces with concentric grooves, as well as to understand experimental results.

We plan to further improve the model by employing several realistic models of reflection that will take into account rough surface and subsurface scattering, perform finite element analysis for the temperature field over the radiating surface of the grooves, as well as incorporate polarization and background radiation effects.

Comparison of results of numerical modeling with measurements of radiation properties of IR calibrators with concentric V-grooves will be described in a follow-on paper.

## REFERENCES

1. R. P. Christensen, G. L. Mehall, S. H. Silverman, et al. "Miniature thermal emission spectrometer for the Mars exploration rovers," *J. Geophys. Research*, **108**, 8064-8066, 2003.
2. X. Xiong, K. Chiang, J. Esposito, B. Guenther, W. Barnes, "MODIS on-orbit calibration and characterization," *Metrologia*, **40**, S89-S92, 2003.
3. S. N. Mekhontsev, V. I. Sapritsky, A. V. Prokhorov, V. B. Khromchenko, M. L. Samoilov, "Modeling, design, and characterization of medium-background blackbodies for full-aperture calibration of spaceborne infrared systems and imagers," *Detectors, Focal Plane Arrays, and Imaging Devices II*, Pingzhi Liang; M. Wigdor; W. G. Frederick, eds., Proc. SPIE, vol. 3553, 247-258, 1998.
4. V. I. Sapritsky, S. N. Mekhontsev, A. V. Prokhorov, K. A. Sudarev, V. B. Khromchenko, M. L. Samoilov, "Precision large-area low- and medium-temperature blackbody sources," *Infrared Spaceborne Remote Sensing VI*, M. S. Scholl, B. F. Andresen, eds., Proc SPIE, vol. 3437 434-445, 1998.
5. R. W. M. Hoogeveen, C. Bernard, F. P. Helmich, et al., "Atmospheric Trace-Gas Measurement with a Balloon-Borne Far Infrared Fabry-Perot Interferometer (SFINX)," *32<sup>nd</sup> ESLAB Symposium: Remote Sensing Methodology for Earth Observation and Planetary Exploration*, ESTEC, Noordwijk, The Netherlands, 1998.
6. J. Ishii, M. Kobayashi, F. Sakuma, "Effective emissivities of black-body cavities with grooved cylinders," *Metrologia*, **35**, 175-180, 1998.
7. L. F. Daws, "The emissivity of a groove," *Brit. J. Appl. Phys.*, **5**, 182-187, 1954.
8. E. M. Sparrow, S. H. Lin, "Absorption of thermal radiation in a V-groove cavity," *Int. J. Heat Mass Transfer*, **5**, 1111-1115, 1962.
9. E. M. Sparrow, J. L. Gregg, "Radiant emission from a parallel-walled groove," *J. Heat Transfer*, **84C**, 270-271, 1962.
10. J. Psarouthakis, "Apparent thermal emissivity from surfaces with multiple V-shaped grooves" *J. Am. Inst. Aeron. and Astron.*, **1**, 1879-1882, 1963.
11. M. Perlmutter, J. Howell, "A Strongly Directional Emitting and Absorbing Surface," *J. Heat Transfer*, **85**, 282-283, 1963.
12. P. F. O'Brien, B. J. Heckert, "Effective Emissivity of a Blackbody Cavity at Nonuniform Temperature," *Illuminating Engineering*, **60**, 187-195, 1965.
13. R. B. Zipin, "The apparent thermal radiation properties of an isothermal V-groove with specularly reflecting walls," *J. Res. NBS*, **70C**, 275-280, 1966.
14. Kelly F. J. "An Equation for the Local Thermal Emissivity at the Vertex of a Diffuse Conical or V-Groove Cavity," *Appl. Opt.*, **5**, 925-927, 1966.
15. Z. Zhimin, "A method for calculating the effective emissivity of a groove structure," *Optical Systems for Space Applications*, Proc. SPIE, vol. 810, 270-277, Hague, The Netherlands, 1987
16. A. V. Prokhorov, S. N. Mekhontsev, L. M. Hanssen, "Emissivity modeling of thermal radiation sources with concentric grooves," *High Temperatures – High Pressures*, **35/36**, 199-207, 2003/2004.
17. Web address: <http://www.virial.com>
18. V. I. Sapritsky, A. V. Prokhorov, "Calculation of the effective emissivities of specular-diffuse cavities by the Monte Carlo method," *Metrologia* **29**, 9-14, 1992.
19. V. I. Sapritsky, A. V. Prokhorov, "Spectral effective emissivities of nonisothermal cavities calculated by the Monte Carlo method," *Appl. Opt.*, **34**, 5645-5652, 1995.
20. A. V. Prokhorov, J. E. Martin, "Monte Carlo simulation of the radiative heat transfer from a blackbody to a cryogenic radiometer," *Optical Radiation Measurements III*, James M. Palmer, ed., Proc. SPIE, vol. 2815, 160-168, Denver, CO, 1995.
21. V. P. Tomaselli, R. Rivera, D. C. Edewaard, K. D. Möller, "Infrared optical constants of black powders determined from reflection measurements," *Appl. Opt.*, **20**, 3961-3967, 1981.
22. Edward D. Palik, ed., *Handbook of Optical Constants II*, 449-460, Academic Press, San Diego, CA, 1998